Nonlinear Dyn (2006) 46:259–272
DOI 10.1007/s11071-006-9041-0

ORIGINAL ARTICLE

Experimental evidence of non-standard bifurcations in non-smooth oscillator dynamics

Paolo Casini · Oliviero Giannini · Fabrizio Vestroni

Received: 12 July 2005 / Accepted: 26 August 2005 / Published online: 8 August 2006

Abstract Analytical and experimental investigations are performed in order to characterize the dynamic behaviour of a non-smooth rotational oscillator, which exhibits multiple discontinuity boundaries in the phase space. The physical system consists of a rotating body subjected to an elastic restoring force and in contact with one or two rough discs rotating with constant driving velocities. The presence of multiple discontinuity boundaries caused by frictional contacts leads to non-standard bifurcations that are studied by means of a simple mechanical model.

A test set-up has then been built to investigate the correctness of modelling of the friction force and the validity of the proposed model for technical applications: the experimental measurements qualitatively and quantitatively capture the basic scenarios anticipated by the model while a strong robustness of the phenomena pointed out by the theoretical analyses has been revealed in the experiments.

Keywords Frictional contacts · Discontinuities · Stick-slip oscillations · Non-standard Bifurcations · Experimental measurements

P. Casini
Dipartimento PRICOS, Università degli Studi di Chieti-Pescara "G. D'Annunzio", Viale Pindaro 42–65127 Pescara, Italy

O. Giannini
Dipartimento di Meccanica e Aeronautica, Università degli Studi di Roma "La Sapienza", Via Eudossiana 18–00184 Roma, Italy

F. Vestroni (✉)
Dipartimento di Ingegneria Strutturale e Geotecnica, Università degli Studi di Roma "La Sapienza", Via Eudossiana 18–00184 Roma, Italy
e-mail: vestroni@uniroma1.it

1. Introduction

Non-smooth characteristics arise in many mechanical systems due to dry friction, impacts, clearances or a combination of these phenomena [1–13]. From a mathematical point of view [14–16], their behaviour is governed by dynamic systems having a different smooth functional form of the vector field in different countable regions of the state space: smoothness in regions of phase space is lost as trajectories cross the boundaries between adjacent regions (*discontinuity boundaries*), where the vector field and its Jacobian can be discontinuous, or even the state vector can be discontinuous. Depending on the properties of the discontinuity boundaries, piecewise smooth dynamic systems (PSS) can be divided into three classes: continuous PSS [4], Filippov PSS [1, 4] and hybrid PSS [4, 15]. In the first class the system vector field is the same in the adjacent regions, whereas its Jacobian changes; in the second class the system vector field changes passing from a region to the adjacent; finally, in the third class the system vector state is discontinuous across a boundary. Examples of continuous PSS

are mechanical systems characterized by discontinuous compliance: namely, oscillators colliding with a deformable stop, block assemblies connected by no-tension springs, beams with breathing cracks. Stick-slip mechanical systems characterized by friction contacts are a widely studied example of Filippov systems [1–4, 17]. Finally, hybrid systems include important applications characterized by impacts, as rocking blocks and oscillators colliding with rigid stops. The mentioned examples are taken from the mechanical field, however, problems concerning PSS are important also in other branches of applied sciences. PSS can exhibit most of the bifurcations exhibited by smooth systems, but in addition they also show novel transitions which will be called *non-standard bifurcations* [7–12, 15, 16].

Particular attention here is focussed on systems exhibiting friction-induced vibrations: in recent years much research effort has been devoted on the theoretical as well as on technical implications of these systems and important experimental studies [2, 13] have been performed dealing with the measurements of friction parameters; nevertheless experimental investigations explicitly devoted to the non-standard bifurcations caused by the presence of multiple frictional contacts are missing.

The model of a non-smooth rotational oscillator, in contact with one or two different rough discs rotating with constant driving velocities, is considered in order to investigate the dynamics of vibrating systems characterized by the occurrence of multiple frictional contacts. Due to the peculiar nonlinearity of the contact force exerted by the two driving supports, the oscillator is modeled by a Filippov PSS, while the presence of multiple discontinuity boundaries leads to non-standard bifurcations governed by interactions between system trajectories and one or both discontinuity boundaries; the evolution of steady state attractors, as the angular velocities of the discs are varied, is studied by means of analytical and experimental investigations.

A test set-up of the model is experimentally investigated in order to verify the accuracy of the friction law used in the model, in order to validate the existence of the non-standard bifurcations predicted by theoretical analyses and hence to check the validity of the proposed model for technical applications.

2. Theoretical model

2.1. System description

The proposed mechanical model is shown in Fig. 1a. A circular sector, of amplitude $\pi + 2\alpha (0 \leq \alpha \leq \pi/2)$, radius R and moment of inertia J_o, can rotate around a point O and is subjected to a visco-elastic restoring force due to a linear rotational spring of stiffness k_R

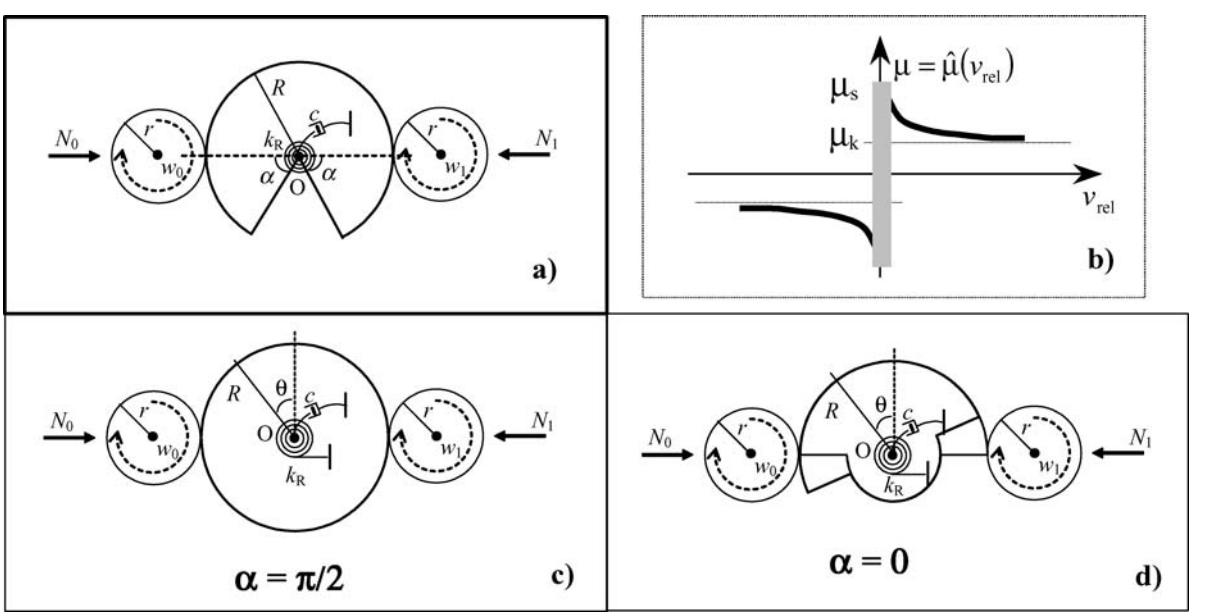

Fig. 1 System model: (a) general scheme; (b) friction law; (c) continuous double contact; (d) sequential contact

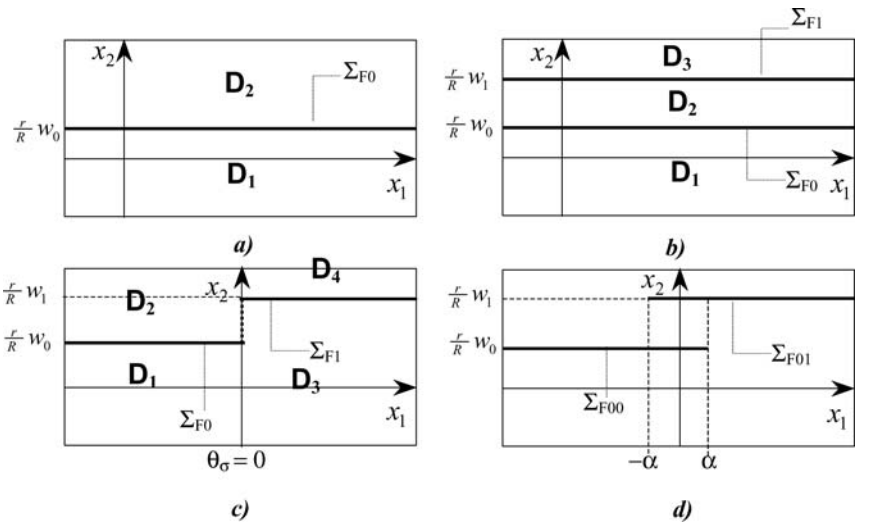

Fig. 2 Discontinuity boundaries in the phase space: (a) continuous contact with a unique disc; (b) continuous double contact with both discs ($\alpha = \frac{\pi}{2}$); (c) sequential contact with only one disc at a time ($\alpha = 0$); (d) Overlapping contact with finite length ($0 < \alpha < \frac{\pi}{2}$)

and to a linearly viscous dashpot of damping coefficient c; its angular rotation θ at the actual time t with respect to the unstressed position is denoted by $x(t)$ which is assumed positive if counterclockwise. The body is dragged by two rough discs (disc 0 and disc 1 both of radius r) rotating with constant driving velocities w_0, w_1 and pushed onto the main disc by constant compressive forces N_0 and N_1 normal to the contact surfaces; unlike the sign convention assumed for the main disc, the angular velocity of the driving discs are assumed positive if clockwise, as shown in Fig. 1a,c,d: this is due to the fact that during the rolling phase main disc and the driving discs will have opposite angular velocities. The driving discs can be characterized by different friction parameters and they can be both in contact with the body depending on the value assumed by α. As it can been easily recognized, if $\alpha = 0$ the body interacts only with one disc at a time, if $\alpha = \pi/2$ the body is continuously in contact with both discs, finally if $0 < \alpha < \pi/2$, during its motion the body can be in contact with only disc 0, with both discs, with only disc 1.

Energy is transferred from the moving supports (disc 0 and/or disc 1) to the rotating oscillator via the friction force which is described by the so-called Conti's friction law; this law, which is widely used in the literature [2, 9, 10], is able to characterize commonly recorded features and provides an hyperbolical dependence on the relative velocity v_{Ri} between the contact points of the body and the disc $i (i = 0, 1)$, as qualitatively sketched in Fig. 1b.

Some important characteristics of the discontinuity boundaries in the phase space, strictly depend on the parameter α. In particular, four classes of systems can be distinguished in which the mass is continuously in contact with at least one disc:

(a) *continuous single contact*: $\alpha = \pi/2$, disc 1 is not in contact. This case, where the mass is continuously in contact only with disc 0, is the simplest one and it will be discussed in order to introduce the basic features of the system behaviour. In the phase space only one discontinuity boundary Σ_{F0} exists, Fig. 2a: the model strictly recalls the case of the well-known 'friction oscillator', widely studied in the literature [2, 3, 6, 8].

(b) *continuous double contact*: $\alpha = \pi/2$ (Figs. 1c and 2b). The mass is continuously in contact with both discs and two distinct discontinuity boundaries, Σ_{F0} and Σ_{F1}, are present in the phase space: these boundaries are placed one upon the other only in the case $w_0 = w_1$.

(c) *sequential contact with only one disc at a time*: $\alpha = 0$ (Figs. 1d and 2c). The mass is in contact only with disc 0 if $x(t) < 0$ and only with disc 1 if $x(t) \geq 0$. Class c) is reduced to class a) if w_0=w_1 and the discs are characterized by the same friction parameters.

(d) *overlapping contact with finite length*: $0 < \alpha < \pi/2$. Depending on the position $x(t)$, the mass interacts either with only one disc at time or with both discs. This is the general case and the relevant switching manifolds are reported in Fig. 2d.

Despite their possible interesting applications, classes (b)–(d), where multiple discontinuity boundaries occur, have not exhaustively been studied in the literature, notwithstanding these classes are felt to likely exhibit a richness of different dynamic behaviours. Many of these phenomena are due to the unique nature of these systems since they depend on the non-smoothness sets of the system and, in particular, on the presence of multiple discontinuity boundaries. These novel phenomena involve generically interactions between system trajectories and phase space discontinuity boundaries. In the following the first three classes will be analytically studied and compared mainly disclosing the dynamic behaviour of class (b) and (c) systems.

2.2. The governing equations: Class a (single disc)

In this case, the oscillator is continuously in contact only with disc 0, since it is assumed that disc 1 is not in contact. The governing equation reads as:

$$J_{\mathrm{O}}\frac{d^2\theta}{dt^2}+c\frac{d\theta}{dt}+k_{\mathrm{R}}\theta-RN_0\mu_0(v_{\mathrm{R}0})=0 \tag{1}$$

The Conti's friction law, relevant to disc 0, reads as follows

$$\mu_0(v_{\mathrm{R}0}):=\frac{\mu_{\mathrm{s}0}-\mu_{\mathrm{k}0}}{1+p_0|v_{\mathrm{R}0}|}+\mu_{\mathrm{k}0} \tag{2}$$

where $v_{\mathrm{R}0}=rw_0-R\frac{d\theta}{dt}$ is the relative velocity between the contact points of the main disc and disc 0 according to the sign conventions given in the previous section, $\mu_{\mathrm{s}0}$ is the static friction coefficient: the friction coefficient hyperbolically decays to a residual value of friction $\mu_{\mathrm{k}0}<\mu_{\mathrm{s}0}$ whereas the coefficient $p_0>1$ quantifies the descent steepness (negative slope) of the friction force. It is now convenient to normalise the equation of motion with respect to the rotary inertia and the stiffness and by introducing a non-dimensional time τ according to the following:

$$\begin{aligned}&\tau=\omega t,\quad \omega=\sqrt{\frac{k_{\mathrm{R}}}{J_0}},\quad \dot{(\circ)}=\frac{d(\circ)}{d\tau}=\frac{d(\circ)}{dt}\frac{1}{\omega},\\ &u_0=\frac{RN_0}{k_{\mathrm{R}}},\quad u_1=\frac{RN_1}{k_{\mathrm{R}}},\quad \zeta=\frac{c}{\sqrt{k_{\mathrm{R}}J_0}}\end{aligned} \tag{3}$$

Then, a state vector $\mathbf{x}\equiv(x_1,x_2)$ gathering the state variables of rotation and absolute angular velocity is defined. In a region $D\subset R^n$ of the phase space the system under investigation can be described as follows, Fig. 2a:

$$\dot{\mathbf{x}}=\begin{cases}\mathbf{f}_1(\mathbf{x};\mathbf{p}), & \text{if } H_{\mathrm{F}0}(\mathbf{x})>0\\ \mathbf{f}_2(\mathbf{x};\mathbf{p}), & \text{if } H_{\mathrm{F}0}(\mathbf{x})<0\end{cases} \tag{4}$$

where:

$$\mathbf{f}_1(\mathbf{x};\mathbf{p})=\begin{cases}x_2\\ -x_1-\zeta x_2+u_0\mu_0(v_{\mathrm{R}0})\end{cases} \tag{5}$$

$$\mathbf{f}_2(\mathbf{x};\mathbf{p})=\begin{cases}x_2\\ -x_1-\zeta x_2-u_0\mu_0(v_{\mathrm{R}0})\end{cases} \tag{6}$$

$\mathbf{p}$ is the parameter vector relevant to damping and friction characteristics, $H_{\mathrm{F}0}$ is a smooth scalar function of the system state

$$H_{\mathrm{F}0}(\mathbf{x}):=rw_0-\omega Rx_2 \tag{7}$$

with nonvanishing gradient $\nabla_{\mathbf{x}}H_{\mathrm{F}0}(\mathbf{x})$ and coinciding with the relative velocity between mass and disc due to the normalizations of Equation (3). $H_{\mathrm{F}0}(\mathbf{x})$ defines the unique switching manifold,

$$\Sigma_{\mathrm{F}0}:=\{\mathbf{x}\in R^n\colon H_{\mathrm{F}0}(\mathbf{x})=0\} \tag{8}$$

The discontinuity boundary $\Sigma_{\mathrm{F}0}$ divides D in the two regions D_1 and D_2 where the system is smooth and is described by the vector fields $\mathbf{f}_1(\mathbf{x};\mathbf{p})$ and $\mathbf{f}_2(\mathbf{x};\mathbf{p})$ respectively, defined over the entire phase space under consideration, i.e., on both sides of $\Sigma_{\mathrm{F}0}$:

$$\begin{cases}D_1:=\{\mathbf{x}\in D\colon H_{\mathrm{F}0}(\mathbf{x})>0\}\\ D_2:=\{\mathbf{x}\in D\colon H_{\mathrm{F}0}(\mathbf{x})<0\}\end{cases} \tag{9}$$

Since the system at hand is a discontinuous PSS, two different vectors, namely $\mathbf{f}_1(\mathbf{x};\mathbf{p})$ and $\mathbf{f}_2(\mathbf{x};\mathbf{p})$, can be associated to a point $\mathbf{x}\in\Sigma_{\mathrm{F}0}$. If the transversal components of $\mathbf{f}_1(\mathbf{x};\mathbf{p})$ and $\mathbf{f}_2(\mathbf{x};\mathbf{p})$ have the same sign, the orbit crosses the boundary and has, at that point, a discontinuity in its tangent vector; the set of this kind of points is called the crossing set $\Sigma^c_{\mathrm{F}0}\subset\Sigma_{\mathrm{F}0}$. On the contrary, if the transversal components of $\mathbf{f}_1(\mathbf{x};\mathbf{p})$

and $\mathbf{f}_2(\mathbf{x};\mathbf{p})$ are of opposite sign, i.e. if the two vector fields are 'pushing' in opposite directions, the state of the system is forced to remain on the boundary and to 'slide' on it. Thus a so-called *sliding motion* takes place; the set of this kind of points is called the sliding set $\Sigma^s_{\mathrm{F0}} \subset \Sigma_{\mathrm{F0}}$ and is the complement to Σ^c_{F0} in Σ_{F0}. It should be noted that in the case of friction discontinuity boundaries, when the above defined sliding motion occurs, a rolling motion occurs between the rotating body and the driving disc and a *sticking phase* is also said to be attained. In other words, the term sliding motion refers to the motion of the state point in the phase space while the term stick phase refers to the motion of the rotating disc.

The solutions of Equation (4) can be constructed by concatenating standard solutions in D_1, D_2 and sliding solutions on Σ_{F0}. The latter ones can be obtained in different ways, e.g. the Filippov's convex method [14] or Utkin's equivalent control method [18]. The governing equations for $\mathbf{x} \in \Sigma^s_{\mathrm{F0}}$ are:

$$\begin{cases} \dot{x}_1 = x_2 \\ \dot{x}_2 = 0 \end{cases}, \quad |-x_1 - \zeta x_2| < u_0 \mu_{\mathrm{s0}} \tag{10}$$

2.3. The governing equations: Class b (continuous double contact)

In this case two different discontinuity boundaries and three smoothness regions do exist in the phase plane: the system can be described as follows, Fig. 2b:

$$\dot{\mathbf{x}} = \begin{cases} \mathbf{f}_1(\mathbf{x};\mathbf{p}), & \text{if } H_{\mathrm{F0}}(\mathbf{x}) > 0 \text{ and } H_{\mathrm{F1}}(\mathbf{x}) > 0 \\ \mathbf{f}_2(\mathbf{x};\mathbf{p}), & \text{if } H_{\mathrm{F0}}(\mathbf{x}) < 0 \text{ and } H_{\mathrm{F1}}(\mathbf{x}) > 0 \\ \mathbf{f}_3(\mathbf{x};\mathbf{p}), & \text{if } H_{\mathrm{F0}}(\mathbf{x}) < 0 \text{ and } H_{\mathrm{F1}}(\mathbf{x}) < 0 \end{cases} \tag{11}$$

where:

$$\mathbf{f}_1(\mathbf{x};\mathbf{p}) = \begin{cases} x_2 \\ -x_1 - \zeta x_2 + u_0\mu_0(v_{\mathrm{R0}}) + u_1\mu_1(v_{\mathrm{R1}}) \end{cases} \tag{12}$$

$$\mathbf{f}_2(\mathbf{x};\mathbf{p}) = \begin{cases} x_2 \\ -x_1 - \zeta x_2 - u_0\mu_0(v_{\mathrm{R0}}) + u_1\mu_1(v_{\mathrm{R1}}) \end{cases} \tag{13}$$

$$\mathbf{f}_3(\mathbf{x};\mathbf{p}) = \begin{cases} x_2 \\ -x_1 - \zeta x_2 - u_0\mu_0(v_{\mathrm{R0}}) - u_1\mu_1(v_{\mathrm{R1}}) \end{cases} \tag{14}$$

H_{F0} and H_{F1} are smooth scalar functions of the system state with nonvanishing gradients:

$$\begin{cases} H_{\mathrm{F0}}(\mathbf{x}) := r w_0 - \omega R x_2 \\ H_{\mathrm{F1}}(\mathbf{x}) := r w_1 - \omega R x_2 \end{cases} \tag{15}$$

As in the previous case, Equations (12)–(14) have been derived by normalising the equations of motion, according to Equation (3). The friction force, relevant to disc $i (i = 0, 1)$ reads as follows:

$$\mu_i(v_{\mathrm{Ri}}) := \frac{\mu_{si} - \mu_{\mathrm{k}i}}{1 + p_i |v_{\mathrm{R}i}|} + \mu_{\mathrm{k}i}, \qquad v_{\mathrm{R}i} := r w_i - \omega R x_2 \tag{16}$$

In Equation (11) $H_{\mathrm{F0}}(\mathbf{x})$ and $H_{\mathrm{F1}}(\mathbf{x})$ define the two discontinuities boundaries:

$$\begin{cases} \Sigma_{\mathrm{F0}} := \{\mathbf{x} \in R^n : H_{\mathrm{F0}}(\mathbf{x}) = 0\} \\ \Sigma_{\mathrm{F1}} := \{x \in R^n : H_{\mathrm{F1}}(\mathbf{x}) = 0\} \end{cases} \tag{17}$$

The discontinuity boundaries Σ_{F0} and Σ_{F1} divide D in the three regions D_i $(i = 1, 2, 3)$

$$\begin{cases} D_1 := \{\mathbf{x} \in D : H_{\mathrm{F0}}(\mathbf{x}) > 0, \quad H_{\mathrm{F1}}(\mathbf{x}) > 0\} \\ D_2 := \{\mathbf{x} \in D : H_{\mathrm{F0}}(\mathbf{x}) < 0, \quad H_{\mathrm{F1}}(\mathbf{x}) > 0\} \\ D_3 := \{\mathbf{x} \in D : H_{\mathrm{F0}}(\mathbf{x}) < 0, \quad H_{\mathrm{F1}}(\mathbf{x}) < 0\} \end{cases} \tag{18}$$

where the system is smooth and is defined by the vector fields $\mathbf{f}_i(\mathbf{x};\mathbf{p})(i = 1, 2, 3)$ which are assumed to be defined over the entire local region of phase space.

In this case too, two different vector $\dot{\mathbf{x}}$ can be associated to points belonging to a discontinuity boundary: namely $\mathbf{f}_1(\mathbf{x};\mathbf{p})$, $\mathbf{f}_2(\mathbf{x};\mathbf{p})$ to $\mathbf{x} \in \Sigma_{\mathrm{F0}}$ and $\mathbf{f}_2(\mathbf{x};\mathbf{p})$, $\mathbf{f}_3(\mathbf{x};\mathbf{p})$ to $\mathbf{x} \in \Sigma_{\mathrm{F1}}$. As it has been done in Subs. 2.2, for each switching manifold the crossing set and the sliding set can be defined: i.e. Σ^c_{F0}, Σ^s_{F0} belonging to Σ_{F0} and Σ^c_{F1}, Σ^s_{F1} belonging to Σ_{F1}. Two sliding motions are possible: a) *sliding motion* in Σ^s_{F0}, when the mass rolls on disc 0, b) *sliding motion* in Σ^s_{F1}, when the mass rolls on disc 1.

Equation (11) can be solved by concatenating standard solutions in D_1, D_2, D_3 and sliding solutions on Σ_{F0} and Σ_{F1}. The governing equations for $\mathbf{x} \in \Sigma^s_{\mathrm{F0}}$ are now:

$$\begin{cases} \dot{x}_1 = x_2 \\ \dot{x}_2 = 0 \end{cases}, \quad |-x_1 - \zeta x_2 + u_1\mu_1(v_{\mathrm{R1}})\,\mathrm{sgn}\,(v_{R1})| < u_0\mu_{\mathrm{s0}} \tag{19}$$

whereas the governing equations for $\mathbf{x} \in \Sigma_{F1}^{s}$ are:

$$\begin{cases} \dot{x}_1 = x_2 \\ \dot{x}_2 = 0 \end{cases}, \quad \begin{aligned} &|-x_1 - \zeta x_2 + u_0\mu_0(v_{R0})\mathrm{sgn}(v_{R0})| \\ &< u_1\mu_{s1} \end{aligned} \tag{20}$$

2.4. The governing equations: class c (sequential contact)

In this configuration the rotating half-disc is in contact with one driving disc at a time: thus the state space exhibits four discontinuity boundaries. By proceeding as in the previous sections, the system can be described as follows, Fig. 2c:

$$\dot{\mathbf{x}} = \begin{cases} \mathbf{f}_1(\mathbf{x};\mathbf{p}), & \text{if } H_{F0}(\mathbf{x}) > 0 \quad \text{and} \quad H_\sigma(\mathbf{x}) < 0 \\ \mathbf{f}_2(\mathbf{x};\mathbf{p}), & \text{if } H_{F0}(\mathbf{x}) < 0 \quad \text{and} \quad H_\sigma(\mathbf{x}) < 0 \\ \mathbf{f}_3(\mathbf{x};\mathbf{p}), & \text{if } H_{F1}(\mathbf{x}) > 0 \quad \text{and} \quad H_\sigma(\mathbf{x}) > 0 \\ \mathbf{f}_4(\mathbf{x};\mathbf{p}), & \text{if } H_{F1}(\mathbf{x}) < 0 \quad \text{and} \quad H_\sigma(\mathbf{x}) > 0 \end{cases} \tag{21}$$

where:

$$\mathbf{f}_{1,2}(\mathbf{x};\mathbf{p}) = \begin{cases} x_2 \\ -x_1 - \zeta x_2 \pm u_0\mu_0(v_{R0}) \end{cases} \tag{22}$$

$$\mathbf{f}_{3,4}(\mathbf{x};\mathbf{p}) = \begin{cases} x_2 \\ -x_1 - \zeta x_2 \pm u_1\mu_1(v_{R1}) \end{cases} \tag{23}$$

In Equation (21) $H_{F0}(\mathbf{x})$, $H_{F1}(\mathbf{x})$ and $H_\sigma(\mathbf{x})$ define three discontinuities boundaries, the last one coinciding with the x_2 axis of the phase plane:

$$\begin{cases} \Sigma_{F0} := \{\mathbf{x} \in R^n : H_{F0}(\mathbf{x}) = 0\} \\ \Sigma_{F1} := \{\mathbf{x} \in R^n : H_{F1}(\mathbf{x}) = 0\} \\ \Sigma_\sigma := \{\mathbf{x} \in R^n : H_\sigma(\mathbf{x}) = 0\} \end{cases} \tag{24}$$

D is then divided in the four regions D_i $(i = 1, 2, 3, 4)$

$$\begin{cases} D_1 := \{\mathbf{x} \in D : H_{F0}(\mathbf{x}) > 0, \quad H_\sigma(\mathbf{x}) < 0\} \\ D_2 := \{\mathbf{x} \in D : H_{F0}(\mathbf{x}) < 0, \quad H_\sigma(\mathbf{x}) < 0\} \\ D_3 := \{\mathbf{x} \in D : H_{F1}(\mathbf{x}) > 0, \quad H_\sigma(\mathbf{x}) > 0\} \\ D_4 := \{\mathbf{x} \in D : H_{F1}(\mathbf{x}) < 0, \quad H_\sigma(\mathbf{x}) > 0\} \end{cases} \tag{25}$$

where the system is smooth and is defined by the vector fields $\mathbf{f}_i(\mathbf{x};\mathbf{p})$ $(i = 1, 2, 3, 4)$ which are assumed to be defined over the entire local region of phase space.

Sliding motions on Σ_{F0} and Σ_{F1} are governed by the following equations:

$$\begin{cases} \dot{x}_1 = x_2 \\ \dot{x}_2 = 0 \end{cases}, \quad |-x_1 - \zeta x_2| < u_0\mu_{s0}$$
$$\begin{cases} \dot{x}_1 = x_2 \\ \dot{x}_2 = 0 \end{cases}, \quad |-x_1 - \zeta x_2| < u_1\mu_{s1} \tag{26}$$

2.5. Characteristic bifurcations exhibited by the model

The previous model exhibits a number of bifurcations with non-standard properties: these have been found and discussed in [9, 10]. Attention is here focused on three characteristic bifurcations disclosed by the model, Figs. 3–5, by varying the velocity of disc 0, w_0, while the velocity of disc 1 is fixed: $w_1 = \bar{w}$.

2.5.1. Sliding-exchange bifurcation in double contact

This behaviour is relevant to a double continuous contact configuration, Fig. 1c. The portraits in Fig. 3 have been obtained by assuming the same friction characteristics for both discs. The bifurcation occurs at $w_0 = w_1 = w_0^\alpha$, when the two discontinuity boundaries are placed one upon the other. The sliding motions in the stable cycle change: in fact, for values of w_0 smaller than w_0^α the stable cycle shows a sliding solution only in Σ_{F0}, i.e. the oscillating disc rolls on disc 0 (Fig. 3a); for values of w_0 larger than w_0^α the stable cycle shows a sliding solution only in Σ_{F1}, i.e. oscillating disc rolls on disc 1 (Fig. 3c). Thus, at $w_0 = w_0^\alpha = \bar{w}$, Fig. 3b, a bifurcation occurs since a sliding solution disappears in Σ_{F1} and appears in Σ_{F0}. This bifurcation is strictly related to the presence of two different discontinuity boundaries and it will be called 'sliding-exchange' bifurcation.

2.5.2. Discontinuous fold bifurcation in double contact

In this case too, the portraits in Fig. 4 have been obtained by considering double contact configuration, Fig. 1c, and by assuming the same friction characteristics for both discs. The bifurcation occurs when $w_0 = w_0^\beta$ Fig. 4b: two periodic solutions, one stable and the other unstable, tangent to Σ_{F1} coexist in the phase

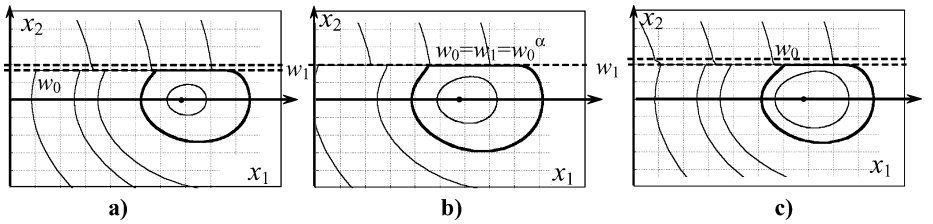

Fig. 3 Phase portraits around the 'sliding-exchange' bifurcation at w_0^{α}; (a) $w_0 < w_0^{\alpha}$, (b) $w_0 = w_0^{\alpha}$, (c) $w_0 > w_0^{\alpha}$

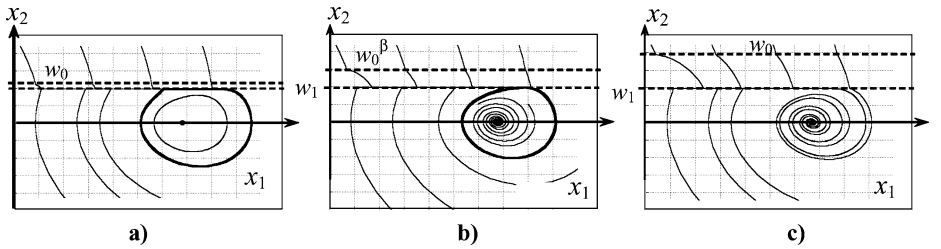

Fig. 4 Phase portraits around the non-smooth fold bifurcation at w_0^{α}; (a) $w_0 < w_0^{\beta}$, (b) $w_0 = w_0^{\beta}$, (c) $w_0 > w_0^{\beta}$

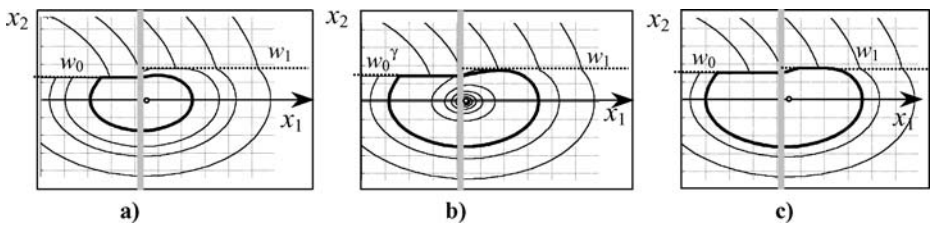

Fig. 5 Phase portraits around the sticking appearance bifurcation at w_0^{γ}; (a) $w_0 < w_0^{\gamma}$, (b) $w_0 = w_0^{\gamma}$, (c) $w_0 > w_0^{\gamma}$

plane, which are a repelling motion for internal points and an attracting motion for external initial conditions. For values of w_0 smaller than w_0^{β} three limit sets exist, Fig. 4a: a stable fixed point, a stable one-sliding Σ_{F1} limit cycle and one unstable zero-sliding limit cycle. The growth of w_0 up to w_0^{β} has a two-fold effect: the amplitude of the unstable cycle increases and the length of the stick phase on belt 1 decreases. For values of w_0 larger than w_0^{β} only a stable fixed point attractor exists: the relevant phase portrait is shown in Fig. 4c. This bifurcation can be classified as a 'discontinuous fold bifurcation' according to the definition given in [8].

2.5.3. Sticking appearance bifurcation in sequential contact

The portraits in Fig. 5 have been obtained by considering sequential contact configuration, Fig. 1d, and by assuming the same friction characteristics for both discs. The bifurcation occurs at $w_0 = w_0^{\gamma}$, Fig. 5b. The sliding motions in the stable cycle change: in fact, for values of w_0 smaller than w_0^{γ} the stable cycle shows one stick phase only on Σ_{F0} (Fig. 5a); for values of w_0 larger than w_0^{γ} a sliding solution on Σ_{F1} is present and the oscillating body rolls sequentially on both discs (Fig. 5c). Thus a bifurcation occurs for $w_0 = w_0^{\gamma}$ since, in the stable cycle, a sliding solution appears on Σ_{F1}.

3. Experiment

The main aim of the experimental campaign is to obtain a qualitative and quantitative confirmation of the peculiar scenarios exhibited by the proposed model. As a first step, the main parameters of the system (e.g. friction coefficients, modal parameters etc.) have been quantified and reported in Section 3.3 and in the Appendix. As a second step, the stick-slip limit cycles obtained for different values of the rotational velocity of the driving discs have been measured for different contact materials.

3.1. Test rig

The experimental rigs, Fig. 6, consist in one oscillating stainless steel disc (D), which represents a one-degree of freedom system that is characterized by the moment of inertia J_o, the rotational stiffness k_R, and the damping coefficient c. The oscillating disc is 25 mm thick and has a diameter of 250 mm, its moment of inertia J is 0.0548 Kg m^2. The two linear springs S_1 and S_2 provide the elastic force that recalls the disc's angular position toward the equilibrium point; the stiffness constant of these springs is 10.5 N/m. The natural frequency of the system can be adjusted changing the spring stiffness.

A test has been performed to measure the resulting rotational stiffness k_R and the damping of the system before starting the stick-slip tests. The first parameter is obtained from a measure of the natural frequency of the oscillating disc, which is 1.1 Hz, leading to a rotational stiffness $k_R = 2.6$ Nm/rad, while the latter, measured from the time decay of the amplitude of free oscillations of the disc, is $c = 0.055$ N ms/rad.

The driving discs (d_0 and d_1) are mounted on two electric DC motors; each motor has a two stages speed reducer. The voltage of the current powering each motor can be adjusted between 2 V and 30 V, allowing the rotational velocity to range between 2 rpm and 26 rpm. To further increase the maximum velocity of the disc's edge, it is possible to change the diameter of the disc. Changing the driving discs, or by adding a coating film around their contact circumference, also allows for the change of the materials in contact. The motors are mounted over a sliding carriage sustained by the two slide bars G. Dead weights provides the force that pushes the driving discs toward the oscillating disc D.

In order to obtain alternate contact between the oscillating disc and the driving disc, some minor modification must be done to the experimental rig: i) the oscillating disc should not be axially symmetric any longer: on its contact surface, along half circumference a patch, obtained from drum brake shoe lining material, is applied (Fig. 6c); ii) an end-stop collar is added to the slide bars, in order to avoid the contact between the rotating and oscillating disc outside of the brake friction material patch.

3.2. Instrumentation

The proposed tests are aimed to characterize how the state-space trajectory of the oscillating disc changes as the velocity of the driving disc changes. In order to measure the state of the oscillating disc two independent measures are taken: a laser telemeter provides the measure of the displacement of the border of the disc that can be easily converted in its angular position, while a relative digital encoder measures the angular velocity of the oscillating disc.

During test the velocity of driving discs are maintained constant. In order to provide that the velocity of driving discs are constant even during the rolling motion, a second encoder was used; in all the cases, the speed variation was found lower than 1%.

Each encoder has 1000 pulse per revolution. In order to obtain a good resolution from the encoder, the software processor of the encoder signals measures both the number of spikes generated by the encoder within the unit time, as well as the average time between two spikes, granting good resolution even for very low angular velocity.

3.3. Friction materials

Experimental tests have been performed with 3 different sets of contact materials, i.e. paper vs. rubber (Figs. 8–10), paper vs. paper (Fig. 11) and drum brake liner vs. rubber (Figs. 12, 13). For each one of these materials the friction law, as a function of the sliding velocity, has been measured.

In order to retrieve the friction law an inverse technique has been used. From a free test the dynamic characteristic of the oscillator is obtained, i.e. the moment of inertia J_o, the rotational stiffness k_R, and the damping coefficient c. The system equation is therefore:

$$J_O \frac{d^2\theta}{dt^2} + c\frac{d\theta}{dt} + k_R\theta = RF(t) \tag{27}$$

where $F(t)$ the sum of the external forces, that is the friction force between the oscillating disc and the rotating disc. Since θ and the angular velocity are measured, while the angular acceleration is obtained by numerical derivation, the time history of the friction force $F(t)$ is the only unknown. From the measurement is then possible to obtain both $F(t)$ and the sliding velocity at the contact $v_R(t)$ and then plot the first as a function of the second (Fig. 7).

The plot shows a first zone for $|v_R| < 0.01\,\mathrm{ms}^{-1}$, characterized by a micro slip between the two materials

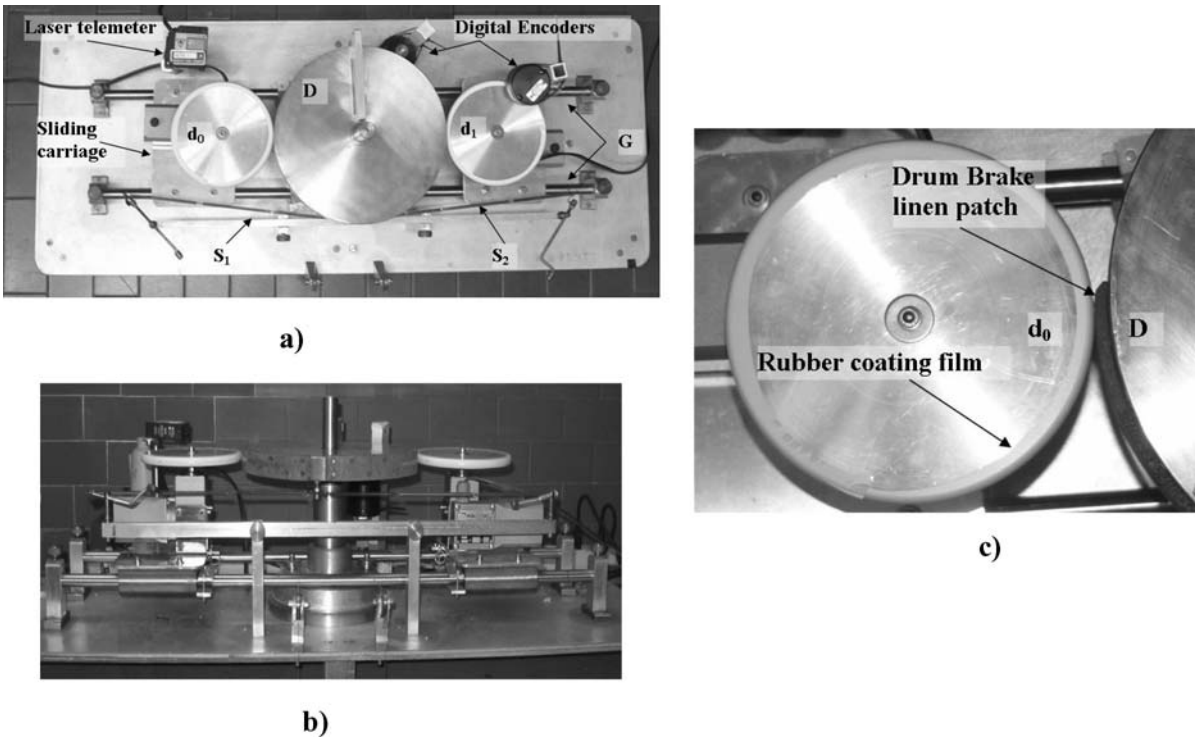

Fig. 6 Experimental set-up: (a) plan view (double contact configuration); (b) front view, (c) detail (sequential contact configuration)

up to the maximum and then exhibits the sliding zone characterized by a decreasing value of the friction coefficient as the sliding velocity increases. The friction force is expressed as a function of the relative velocity as:

$$F(t) = F(v_{\mathrm{R}}(t)) = N\left(\frac{\mu_{\mathrm{s}} - \mu_{\mathrm{k}}}{1 + p|v_{\mathrm{R}}|} + \mu_{\mathrm{k}}\right) \tag{28}$$

where N is the normal force, applied by the dead weight to the carriage supporting the disc. From the measurements it is then possible to fit the experimental data with the proposed friction model in order to obtain the best values for the three unknown parameters μ_{s}, μ_{k}, and p as shown in Table 1. The resulting friction force is plotted in figure as a grey line.

Table 1 Estimated values of the friction law parameters

	Paper vs. paper	Drum brake liner vs rubber	Paper vs. rubber
μ_{s}	0.35	0.5	0.65
μ_{k}	0.25	0.33	0.35
p	15	20	15

3.4. Test procedure

The output of the measure is the state-space trajectory of the oscillating disc. Each set of measurements is characterized by the normal force, the contact materials (coating of the discs), and the velocity of the first driving disc, the one with fixed angular velocity. Each measure within a set is characterized by the angular velocity of the second driving disc that ranges from 2 rpm, its lower limit, to 26 rpm, its upper limit. Within a set of measurements, the velocity of the second disc is changed randomly within the range, to avoid systematic error due the wear of the contact surface.

The stick-slip measures consist of a 20 s acquisition of the data by the laser telemeter and the digital encoders. It is useful to wait between the beginning of the oscillation of the disc and the actual start of the measure, up to 5 s to avoid transitory behaviour: in this time the system usually reaches a steady limit cycle which is measured.

A further refinement of the acquired interval is possible during the post processing, when the time bounds of the measurement can be redefined to cut out non-consistent behaviour.

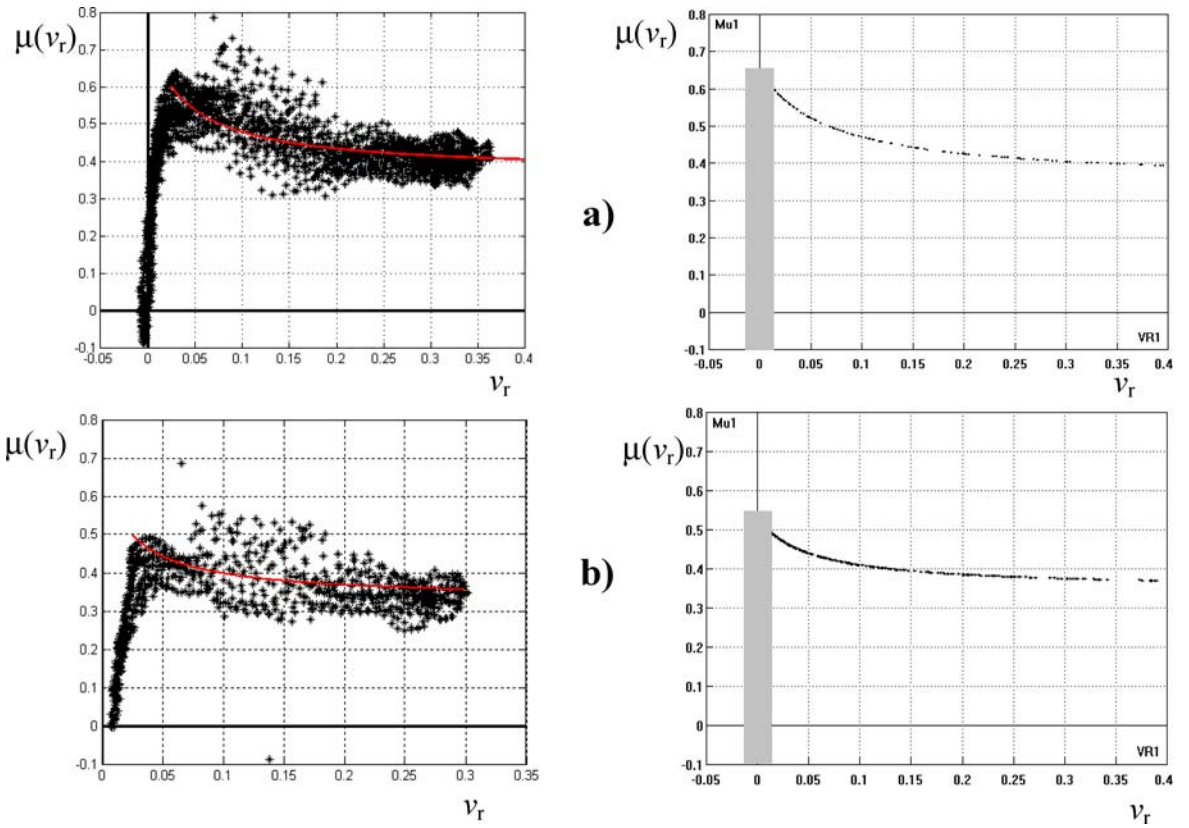

Fig. 7 Experimental and identified friction laws: (a) rubber-paper; (b) rubber- brake patch

4. Experimental results and comparisons

As shown in the previous Section, the system behaviour of the nonsmooth oscillator has been measured under different conditions: the comparison of numerical simulations using the identified friction characteristics in Subsection 3.3 with the measured system behaviour shows a good agreement and gives a verification of the theoretical model proposed in Section 2.

4.1. Double contact

4.1.1. Sliding-exchange bifurcation

The relevant theoretical basis for this kind of bifurcation has been recalled in Subsection 2.5. The same behaviour has been experimentally reproduced and measured, considering a contact pair rubber vs. paper for both discs. The measured friction characteristics are reported in Fig. 7a while the measured phase portraits are shown in Figs. 8, where disc 1 is kept at fixed angular velocity $w_1 = 0.83$ rad/s, while the velocity of disc 0 varies from 0.41 (Fig. 8a) to 1.4 rad/s (Fig. 8f); the predicted sliding-exchange bifurcation occurs at $w_0 = 0.83$ rad/s, as shown in Fig. 8c. Figures 9 report the comparison of the previous measured response with the theoretical model with the identified friction characteristics: the agreement is very good and the basic phenomenological aspects are captured qualitatively and quantitatively by the theoretical model.

The only difference between measured and numerical response is related to the small oscillation that the experiments show at the slip-stick transition and that is revealed by a small protuberance in the measured phase plane just before entering the stick phase. These oscillations consistently precede the stick phase when rubber is present, Figs. 9, 10, 12, 13, while are not revealed in the other cases studied in absence of rubber, Fig. 11. Indeed they are probably related to the microslip due to elastic contact force and are not really

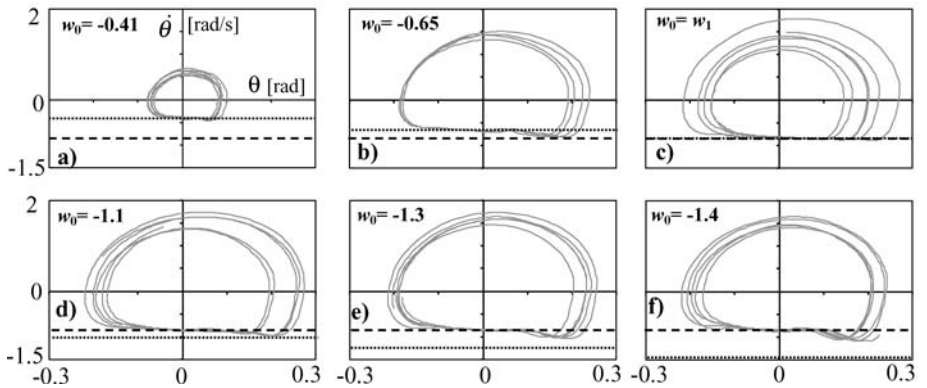

Fig. 8 Experimental phase portraits around the sliding exchange bifurcation. $w_1 = -0.83$ rad/s

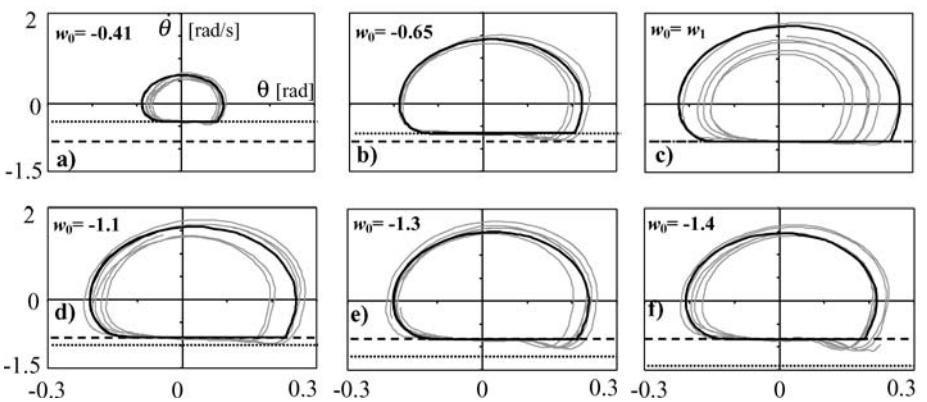

Fig. 9 Phase portraits around the sliding exchange bifurcation: model (—) and experiments (.....). $w_1 = -0.83$ rad/s

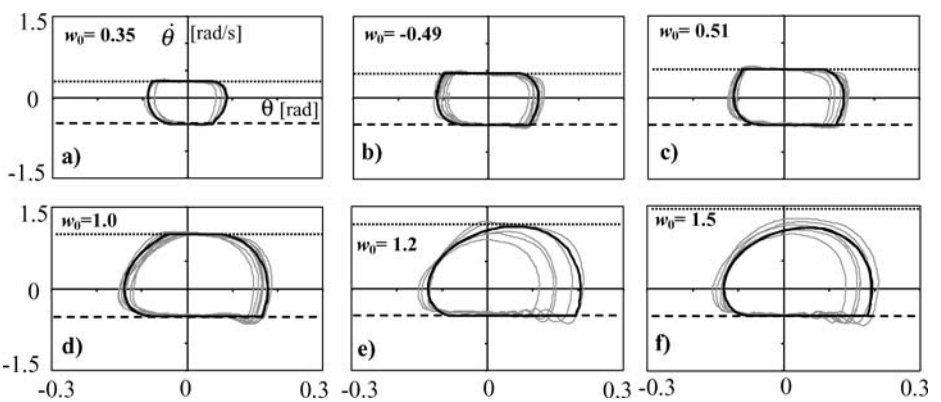

Fig. 10 Phase portraits around the sticking disappearance bifurcation: model (—) and experiments (.....). $w_1 = -0.5$ rad/s

oscillations in the friction force since gross slip is no longer taking place.

4.1.2. Sticking disappearance bifurcation

This kind of bifurcation, predicted by the theoretical analysis as shown in Subsection 2.5, has been experimentally obtained when the discs rotate with discordant angular velocities and the same contact materials of the previous case have been considered. The measured friction characteristics are reported in Fig. 7a while the measured phase portraits are shown in Fig. 10, where disc 1 is kept at fixed angular velocity $w_1 = -0.5$ rad/s and the velocity of disc 0

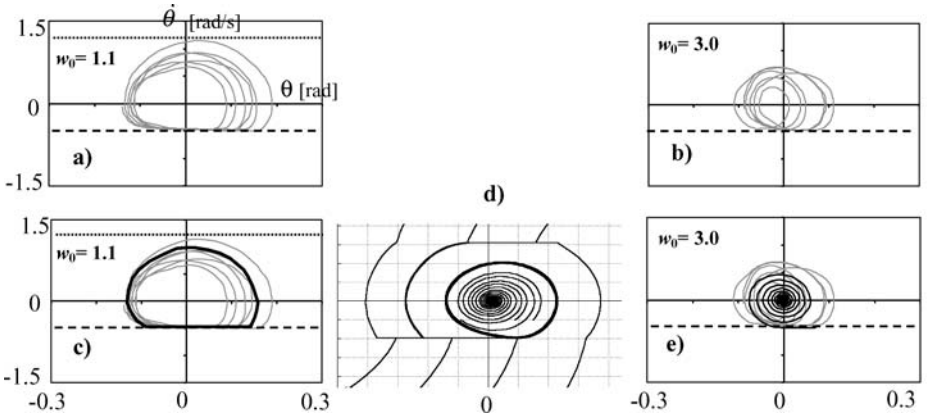

Fig. 11 Phase portraits around the nonsmooth fold bifurcation: model (—) and experiments (.....). $w_1 = -0.5$ rad/s

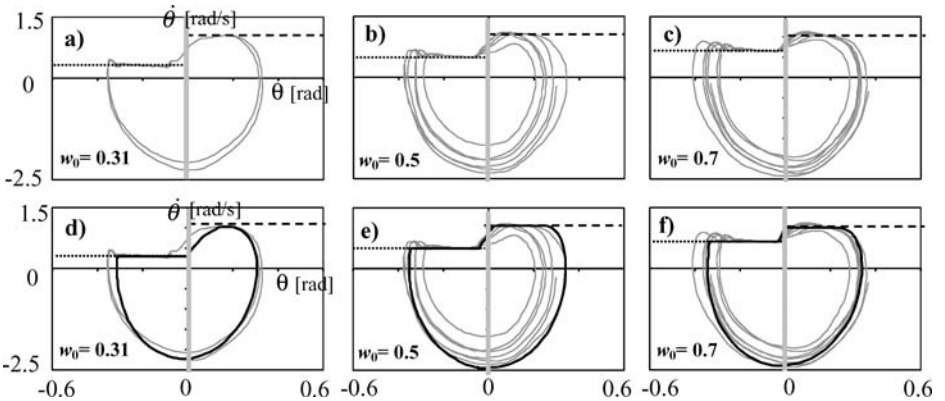

Fig. 12 Phase portraits around the sticking appearance bifurcation: model (—) and experiments (.....). $w_1 = 1.0$ rad/s

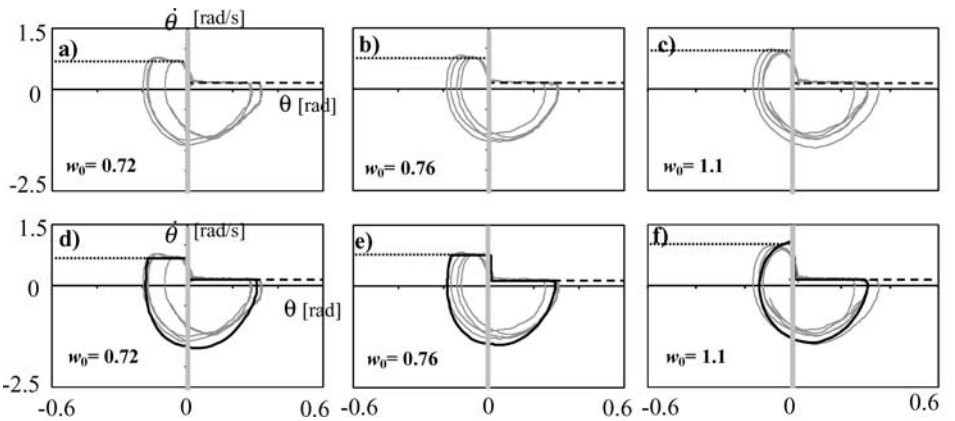

Fig. 13 Phase portraits around the sticking appearance bifurcation: model (—) and experiments (.....). $w_1 = 1.15$ rad/s

varies from 0.35 (Fig. 10a) to 1.5 rad/s (Fig. 10f); the predicted bifurcation occurs around $w_0 = 1.2$ rad/s, where the measured stable cycle becomes tangent to Σ_{F0} and the stick phase is no longer present in Σ_{F0}. In this case too comparison with the numerical results, which has been reported in the same figure by a thick line, confirms the accuracy of the proposed model.

4.1.3. Non-smooth fold bifurcation

In this case the relevant theoretical basis has been recalled in Subsection 2.5 and the same behaviour has been experimentally reproduced and measured when the discs rotate with discordant angular velocities and a contact pair paper vs. paper for both discs is considered. The measured friction characteristics are reported in Table 1 while the measured phase portraits are shown in Fig. 11a,b, where disc 1 is kept at fixed angular velocity $w_1 = -0.5$ rad/s, while the velocity of disc 0 varies from 1.1 (Fig. 11a) to values higher than 2 rad/s (Fig. 11b); Figures 11c,e shows the comparisons with numerical results: it should be noted that the predicted bifurcation can be captured uniquely by the theoretical model, Fig. 11c, since the trajectory becomes unstable. The scenario with only one stable fixed point in the phase plane is shown in Figs. 11b, e: the measured phase portrait is not characterized simply by a 'point' but consists of small oscillations around the fixed point: unlike the previous scenarios, here the imperfections in the real system and the inability of the set-up prevent a better description of the phase portrait.

4.2. Sequential contact

Sequential contact configuration has been then considered for experimental purposes.

4.2.1. Sticking-appearance and sticking disappearance bifurcations

These non-standard bifurcations, theoretically described in Subsection 2.5, have been experimentally reproduced and measured when a contact pair rubber vs. drum brake linen for both discs is considered, Fig. 7b. As far as sticking appearance bifurcation is concerned, Fig. 12a,b,c show the measured phase portraits whereas Fig. 12d,e,f report the relevant comparisons with the model.

The sticking-disappearance bifurcation is described at the same way by Fig. 13. This last bifurcation, occurs at $w_0 = 1.1$ rad/s (Fig. 13b,f) and it is basically similar to the one experimentally reported by Fig. 10e for the double contact configuration.

In both cases, a good qualitative and quantitative agreement is observed, the only difference being the changeover at $\theta = 0$ when one driving disc replaces the other: in the model this change is quite sudden while in the physical prototype it occurs gradually and it is accompanied by small oscillations. Notwithstanding these phenomena the predicted bifurcations exhibit a strong robustness and are well captured by the model.

5. Conclusions

The model of a non-smooth rotational oscillator, which exhibits multiple discontinuity boundaries in the phase space, is considered in order to investigate the dynamics of vibrating systems characterized by the occurrence of multiple frictional contacts. The dynamics of the model are of interest because it is a simple representation of mechanical systems with multiple non-smooth characteristics and at the same time its response exhibits non-classical bifurcation scenarios as a consequence of the occurrence of multiple discontinuity boundaries caused by the disc contacts.

Particular attention has been devoted to three different bifurcations disclosed by the theoretical analyses: (i) non-smooth fold bifurcation, which divides a scenario with one fixed point from another with three co-existing solutions; (ii) sliding-exchange bifurcation, when the trajectory has a stick phase on one driving disc and then on the other; (iii) sliding bifurcations, characterized by abrupt appearance, or disappearance, of one or multiple stick phases in the trajectories.

An experimental rig has been built and its behaviour is experimentally investigated: the accuracy of the friction law used in the model has been verified and the relevant friction parameters have been identified; furthermore, the existence of the non-standard bifurcations predicted by the theoretical analyses has been confirmed.

Based on the performed measurements, a good qualitative and quantitative agreement with the numerical results furnished by the model with identified friction parameters has been observed: the non-standard bifurcations predicted by the model are revealed throughout the experiments under different schemes independent of the contact materials involved. The robustness of these phenomena is important, since in technical applications the friction parameters may vary considerably, and frequently they are not known at all. Thus, the analytical and experimental investigations, though limited to this simple model, could provide a valuable insight on the basic features exhibited by more complex mechanical systems with non-smooth

characteristics related to the presence of multiple frictional contacts.

Appendix: System parameters

Oscillating Disc

Material: stainless steel.
Density: $\rho = 7800\,\mathrm{Kg/m^3}$.
Mass: $m = 9.57\,\mathrm{Kg}$, *Radius*: $R = 0.125\,\mathrm{m}$.
Thickness: $s = 0.025\,\mathrm{m}$.
Moment of inertia: $J_\mathrm{o} = 0.0548\,\mathrm{Kg\,m^2}$.
Rotational stiffness: $k_\mathrm{R} = 2.62\,\mathrm{Nm/rad}$.
Natural frequency: $f_\mathrm{n} = 1.1\,\mathrm{Hz}$.
Damping: $c = 0.055\,\mathrm{N\,m\,s/rad}$

Driving Discs

Rotational velocity range: $2.5\,\mathrm{rpm} < n < 26\,\mathrm{rpm}$
Radius: $r = 0.06\,\mathrm{m}$;
Velocity range at the edge: $0.019\,\mathrm{m/s} < v < 0.16\,\mathrm{m/s}$

References

1. Shaw, S.H.: On the dynamic response of a system with dry friction. J. Sound Vib. **108**(2), 305–325 (1986)
2. Popp, K., Hinrichs, N., Oestreich, M.: Analysis of a self-excited friction oscillator with external excitation. In: Dynamics with Friction, Guran, A., Pfeiffer, F., Popp, K. (eds.), World Scientific, London (1996)
3. Galvanetto, U., Bishop, S.R.: Dynamics of a simple damped oscillator undergoing stick-slip vibrations. Meccanica **34**, 337–347 (1999)
4. Leine R.I.: Bifurcations in Discontinuous Mechanical Systems of Filippov-type, PhD Thesis, Technische Universiteit Eindhoven (2000)
5. Pfeiffer, F., Glocker, Ch.: Contacts in multibody systems. J. Appl. Math. Mech. **64**(5), 773–782 (2001)
6. Andreaus, U., Casini, P.: Dynamics of friction oscillators excited by moving base or/and driving force. J. Sound Vib. **245**(4), 685–699 (2001)
7. Leine, R.I., van Campen, D.H., De Kraker, A., van Den Steen, L.: Stick-slip vibration induced by alternate friction models. Nonl. Dyn. **16**, 41–54 (1998)
8. Galvanetto, U.: An example of a non-smooth fold bifurcation. Meccanica **36**, 229–233 (2001)
9. Casini, P., Vestroni, F.: Nonsmooth dynamics of a double-belt friction oscillator. In: IUTAM Symposium on Chaotic Dynamics, Roma 8–13 Giugno, 253–262 (2003)
10. Casini, P., Vestroni, F.: Nonstandard bifurcations in mechanical systems with multiple discontinuity boundaries. Nonl. Dyn. **35**(1), 41–59 (2004)
11. Casini, P., Vestroni, F.: Bifurcations in hybrid mechanical systems with discontinuity boundaries. Int. J. Bif. Chaos **15**(6), 2003–2013 (2005)
12. Luo, A.C.J., Chen, L.: Periodic motions and grazing in a harmonically forced, piecewise, linear oscillator with impacts. Chaos Solitons Fractals **24**, 567–578 (2005)
13. Ko, P.L., Taponat, M.C., Pfaifer, R.: Friction-induced vibration with and without external disturbances. Tribol. Int. **34**, 7–24 (2001)
14. Filippov, A. F.: Differential Equations with Discontinuous Righthand Sides, Kluwer Academic Publishers, Dordrecht, The Netherlands (1988)
15. Di Bernardo, M., Johansson, K.H., Vasca, F.: Self-Oscillations in relay feedback systems: symmetry and bifurcations. Int. J. Bif. Chaos **11**(4), 1121–1140 (2001)
16. Di Bernardo, M., Budd, C.J., Champneys, A.R.: Unified framework for the analysis of grazing and border-collisions in piecewise-smooth systems. Phys. Rev. Lett. **86**, 2554–2556 (2001)
17. Awrejcewicz, J., Holicke, M.M.: Melnikov's method and stick-slip chaotic oscillations in very weakly forced mechanical systems. Int. J. Bif. Chaos **9**, 505–518 (1999)
18. Utkin, V.I.: Sliding Modes in Control Optimization, Springer Verlag, Berlin (1992)